RSC Advances

PAPER

View Article Online
View Journal | View Issue

Cite this: *RSC Adv.*, 2026, **16**, 18061

Design, synthesis and biological evaluation of tacrine-sulphonamide hybrids as a potent acetylcholinesterase inhibitor

Mangari Madhusudhan Reddy,[a] Eeda Koti Reddy,[a] Abhithaj J,[b] Radul R. Dev,[b] V. S. Nagarajesh Kadambari[a] and Shaik Anwar *[a]

Received 2nd February 2026
Accepted 20th May 2026

DOI: 10.1039/d6ra00900j

rsc.li/rsc-advances

Novel tacrine-based sulphonamide derivatives were designed and evaluated for their ability to inhibit acetylcholinesterase (AChE) using molecular docking and *in vitro* assays. Docking studies revealed strong interactions with key active-site residues, including Trp86, Trp286, Tyr337, and Phe338, mediated through π–π stacking, π-cation interactions, hydrogen bonding, and hydrophobic contacts. Among the synthesized compounds, **6g**, **6i**, **6j**, and **6k** exhibited superior binding affinities, with compound **6j** demonstrating the highest docking score of −9.18 kcal mol^{-1} and a binding energy of −97.92 kcal mol^{-1}. *In vitro* screening using Ellman's method confirmed potent AChE inhibition, with IC_{50} values in the nanomolar range. Structure–activity relationship analysis indicated that methyl-substituted piperidine derivatives significantly enhanced inhibitory potency, with compounds **6j** and **6k** achieving IC_{50} values of 7.40 nM and 11.33 nM, respectively.

Introduction

Alzheimer's disease (AD) is a progressive neurodegenerative disorder and the leading cause of dementia worldwide, accounting for approximately 60–70% of all dementia cases.[1] Pathologically, AD is characterized by the accumulation of extracellular amyloid-beta (Aβ) plaques and intracellular neurofibrillary tangles composed of hyperphosphorylated tau protein. These hallmark lesions disrupt synaptic function, impair neuronal communication, and ultimately lead to widespread neuronal death and brain atrophy.[2] Clinically, AD primarily affects individuals over the age of 65 and manifests as a gradual decline in cognitive abilities, including memory loss, impaired judgment, language deficits, and behavioural disturbances such as apathy, agitation, and depression.[3,4]

The burden of AD is immense and continues to grow; every three seconds, someone, somewhere, develops dementia. In 2019, approximately 55 million people worldwide were estimated to be living with dementia, a figure projected by the World Health Organization (WHO) to rise to 139 million by 2050 due to aging populations and increased life expectancy.[5] This alarming trend underscores the urgent need for effective therapeutic strategies, early diagnostic tools, and coordinated global public health initiatives to mitigate the impact of AD on individuals, families, and healthcare systems.

Acetylcholinesterase (AChE) is a crucial biochemical enzyme that regulates acetylcholine-mediated neuronal transmission in the central nervous system.[6] It possesses a distinctive structure featuring two binding sites connected by a narrow gorge region and has historically served as a primary pharmacological target for the treatment of Alzheimer's disease.[7] AChE catalyzes the hydrolysis of acetylcholine (ACh) into choline and acetate, thereby terminating ACh-mediated synaptic transmission in the central nervous system (CNS) with exceptionally high catalytic efficiency. Structurally, AChE comprises three key features: the catalytic active site (CAS), the gorge, and the peripheral anionic site (PAS). The gorge region connects the CAS to the PAS and the enzyme surface.[8,9]

Tacrine, the first acetylcholinesterase inhibitor (AChEI) approved for clinical use in the treatment of Alzheimer's disease, marked a significant milestone in neurodegenerative therapeutics. Despite its eventual withdrawal from the market due to dose-dependent hepatotoxicity, in recent years, numerous multifunctional tacrine-based compounds have been synthesized, retaining their acetylcholinesterase (AChE) inhibitory properties. Earlier studies explored various hybrid molecules derived from tacrine, aiming to enhance their therapeutic potential. Researchers are concentrating on various tacrine derivatives, including tacrine-2-amide derivatives,[10a] tacrine-melatonin molecule.[10b] donepezil-tacrine scaffold,[10c] tacrine-caffeic acid hybrids[10d], tacrine-8-hydroxy quinoline hybrids,[10e] Cyst amine-tacrine-dimer,[10f] tacrine-melatonin molecule,[10g] bis-tacrine's,[10h] pyrano-tacrines,[10i] pyrano[2,3-*c*] pyrazole-tacrine

[a]*Department of Chemistry, School of Applied Science and Humanities, Vignan's Foundation for Science, Technology and Research-VFSTR, Vadlamudi, Guntur 522213, Andhra Pradesh, India. E-mail: shaikanwarcu@gmail.com; drsa_sh@vignan.ac.in; Tel: (+91)-8632344700*

[b]*Centre for Integrative Omics Data Science (CIODS), Yenepoya (Deemed to Be University), Mangalore, Karnataka 575018, India*

hybrids,[10j] tacrine-lophine hybrids,[10k] quinone-tacrine hybrids,[10l] NO-donor-tacrine hybrids,[10m] are few examples, despite its limitations, it continues to serve as a key framework in efforts to design and develop innovative acetylcholinesterase (AChE) inhibitors, tacrine remains a foundational scaffold in medicinal chemistry for the design of novel AChEIs.[11] Its well-characterized pharmacophore and ability to interact with both the catalytic active site (CAS) and the peripheral anionic site (PAS) of AChE make it an attractive core structure for the development of multitarget-directed ligands (MTDLs). This review provides a comprehensive overview of tacrine-based MTDLs reported in the literature since 2015, with a particular focus on merged hybrid compounds in which tacrine is structurally integrated with a second pharmacophore to enhance therapeutic efficacy and broaden biological activity.[12,18–26]

The molecular architecture of these novel hybrids was based on a dual-binding strategy designed to exploit the synergistic potential of established acetylcholinesterase (AChE) inhibitors, tacrine and donepezil, together with pharmacologically versatile sulfonamide scaffolds. Tacrine is a potent AChE inhibitor, but its clinical utility is limited by hepatotoxicity. Hybridization with sulfonamides, a class known for antimicrobial and neuroprotective properties, offers a promising avenue for enhanced efficacy and safety. Molecular modeling and kinetic studies indicate that these hybrid ligands effectively span the 20 Å length of the AChE enzymatic gorge.[13,14]

In the tacrine-sulfonamide series, the tacrine moiety anchors within the catalytic active site (CAS) *via* π–π stacking with Trp84 and Phe330, while the sulfonamide group extends toward the peripheral anionic site (PAS), stabilized by hydrogen bonding with Tyr70 or Asp72. Structure–activity relationship (SAR) analysis identified the six-membered ring system as the optimal scaffold, with the most potent derivative achieving an IC_{50} of 0.009 μM-representing a six-fold increase (Fig. 1) in potency over tacrine and a 220-fold increase over galantamine.[15,17]

In parallel, a series of aryl-sulfonamide-donepezil hybrids yielded a standout lead compound. Structurally, this molecule integrates the benzyl-piperidine pharmacophore of donepezil with a biphenyl-sulfonamide moiety through a single-carbon linker ($n = 1$). This lead exhibited an IC_{50} of 1.6 μM against AChE and demonstrated robust inhibition (60.7%) of self-induced amyloid-β aggregation, thereby validating sulfonamide hybridization as a high-impact strategy for developing multifunctional agents against neurodegenerative pathology.[13,16]

The synthesis of these hybrid compounds typically involves modular strategies using readily available starting materials,

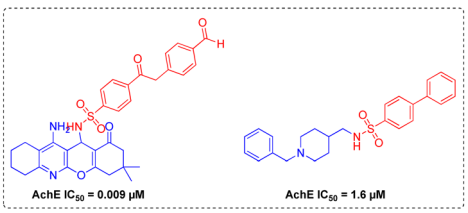

Fig. 1 Biologically active tacrine-sulfonamide hybrid derivatives.[13,15]

Fig. 2 Biologically active tacrine-2 amides and its derivatives.

enabling structural diversity and systematic optimization. Their acetylcholinesterase inhibition profiles are evaluated in comparison with tacrine, and detailed structure–activity relationship (SAR) analyses are presented to identify key molecular features contributing to potency, selectivity, and reduced toxicity. Where applicable, molecular modelling and docking studies are included to elucidate binding interactions within the AChE active site, highlighting the roles of π–π stacking, hydrogen bonding, and hydrophobic contacts in stabilizing the enzyme-inhibitor complex.[27,28]

Traditionally, most research on tacrine derivatives has focused on amine substitutions. In contrast, our earlier studies explored modifications at the C2 position of the cyclohexyl ring and the C6 position of the aromatic ring of tacrine. We found that C2-substituted tacrine derivatives, known as tacrine-2-amides (Fig. 2), interact effectively with the peripheral anionic site (PAS) of acetylcholinesterase (AChE). Our previous work demonstrated that tacrine-2-amides with a three-carbon linker exhibited strong AChE inhibition ($IC_{50} = 5.17$ nM), while a 6-bromo tacrine-2-amide with the same linker length showed comparable activity ($IC_{50} = 7.14$ nM).[29–34]

In the present study, we extend this research by evaluating tacrine-2-sulphonamide derivatives. We also assess their cholinesterase inhibitory activity, physicochemical properties, and molecular binding interactions.

Results and discussion

A series of novel tacrine-sulfonyl piperazine derivatives was synthesized using commercially available starting materials.

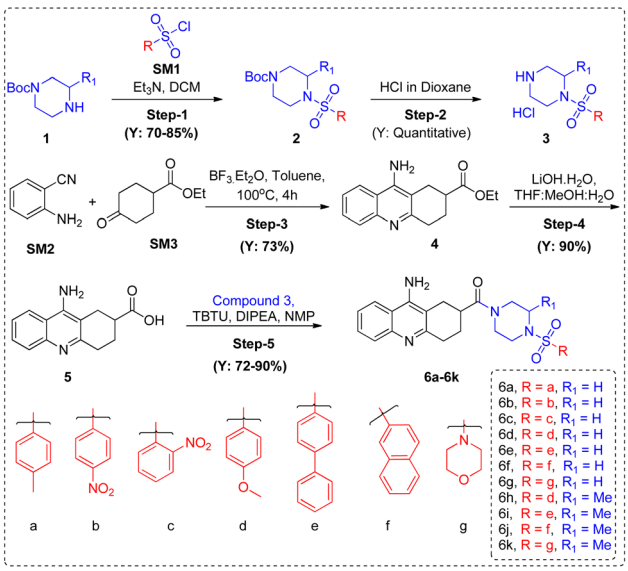

Scheme 1 Substrate scope of tacrine **6a–6k**.

The synthetic route involved three key steps (Scheme 1): (i) sulfonylation to form a sulphonamide bond between sulfonyl chlorides (**1**) and the Boc-protected piperazine (**2**) to obtain intermediate **3**; (ii) Boc deprotection of the *N*-Boc piperazine using 4 M HCl in 1, 4-dioxane to yield intermediate **4**; and (iii) acid-amine coupling with tacrine-2-acid using TBTU as the coupling reagent and DIPEA as the base in NMP as the solvent. This sequence resulted in the formation of eleven final compounds (**6a–6k**) in good yields. The structures of these derivatives were confirmed by ^{1}H NMR, ^{13}C NMR, and HRMS.

Molecular docking

The three-dimensional structure of recombinant human acetylcholinesterase (hAChE) complexed with donepezil (PDB ID: 4EY7) was retrieved from the Protein Data Bank (PDB) and prepared using the Protein Preparation Wizard in the Schrödinger Suite. Preprocessing steps included the removal of crystallographic water molecules, correction of structural anomalies, and proper assignment of bond orders, hydrogen atoms, disulfide bridges, and zero-order bonds for coordinated metal ions. During the refinement phase, missing side-chain atoms were added to complete the protein model.[31] Energy minimization was performed using the OPLS_4 force field to resolve steric clashes present in the original PDB structure, employing an all-atom restrained minimization protocol.

Following optimization of the protein structure, receptor grid generation was carried out by defining a cubic grid box (~20 Å) centered on the coordinates of the co-crystallized ligand to accurately represent the binding site. Tacrine-based sulphonamide derivatives were designed, and their structures were drawn using ChemSketch or ChemDraw. The ligands were then prepared and optimized using the LigPrep module. Ionization states were generated with the Epik module at physiological pH, incorporating all possible tautomers and stereoisomers. Energy minimization of the optimized ligand structures was performed using the OPLS_4 force field.[35]

In addition to these derivatives, the 3D structures of tacrine and donepezil (the co-crystallized ligand, extracted from the prepared hAChE structure) were also optimized for validation and comparison. The AChE active site comprises five key regions: the oxyanion hole (Gly121, Gly122, Ala201), the catalytic triad (Ser203, His447, Glu334), the choline-binding site (Trp84, Tyr133, Tyr337, Phe330), the acyl-binding pocket (Phe295, Phe297, Asp74, Trp279, Phe330, Tyr70), and the peripheral anionic site (PAS) (Tyr70, Trp295, Phe330). The PAS plays a critical role in modulating amyloid-β (Aβ) fibril aggregation, and inhibitors targeting this region have been shown to reduce Aβ aggregation and enhance peptide clearance more effectively than those binding solely to the catalytic triad.[36,37]

Tacrine and donepezil were docked for comparison, as they are commonly used as positive controls *in vitro* acetylcholinesterase (AChE) assays, and their binding energies are summarized in Table 1. Tacrine exhibited a Glide score of −10.59 kcal mol^{-1} and a binding energy of −54.02 kcal mol^{-1}. Its interaction with AChE was stabilized by π–π stacking interactions with Tyr341 and π-cation interactions with Tyr337 and Trp86. Donepezil showed a Glide score of −10.57 kcal mol^{-1} and a stronger binding energy of −97.4 kcal mol^{-1}, forming π–π interactions with Trp86 and Trp286, and π-cation interactions with Tyr337, Phe338, and Phe295.

Among the designed tacrine-sulphonamide derivatives, compound **6j** displayed good affinity for AChE, with a Glide score of −9.18 kcal mol^{-1} and a binding energy of −97.98 kcal mol^{-1}. It formed two π–π interactions with Trp286 and two strong hydrogen bonds with Ala343. Compound **6g** also showed notable affinity, with a Glide score of −7.82 kcal mol^{-1} and a binding energy of −94.79 kcal mol^{-1}, exhibiting π–π interactions with Trp86 and π-cation interactions with Trp86, Tyr337, and Phe338, similar to the interaction profile of donepezil. Compound **6k** had a Glide score of −6.97 kcal mol^{-1} and a binding energy of −90.65 kcal mol^{-1}, forming π–π interactions with Trp286 and hydrogen bonds with Tyr72 and Phe295. Additionally, compound **6i** demonstrated strong hydrogen bonding interactions with Tyr124 and Ser125.

The binding affinities of these compounds were further stabilized by van der Waals contacts and hydrophobic interactions with residues lining the active site, including Trp86, Gly120, Gly122, Tyr124, Val294, Phe295, Phe297, Phe338, and Tyr341, which are key residues of the PAS.[38,39] These hydrophobic interactions contributed significantly to the overall binding stability.

Overall, molecular docking studies revealed that binding was stabilized through a combination of stacking interactions (π–π

Table 1 Ligand interaction diagram showing tacrine derivatives at the active center of ACh

S.No.	Compound name	Glide score (kcal mol^{-1})	Binding energy (kcal mol^{-1})	Interactions
1	**6a**	−5.84	−47.68	TRP286, TYR124 and ARG296
2	**6d**	−5.29	−43.25	TYR124 2HBonds
3	**6e**	−1.33	−64.98	TRP286, SER125 1HBond
4	**6g**	−7.82	−94.79	TRP86, TRP86, TYR337 and PHE338, 1 HBond in PHE295
5	**6h**	−7.66	−23.96	TRP286, HIS447, a HBond interaction at GLY122
6	**6i**	−3.55	−81.28	TYR124, SER125 have HBond interaction
7	**6j**	−9.18	−97.92	TRP286 pi–pi interaction, HBond at ALA343
8	**6k**	−6.97	−90.65	TRP286, TYR72 and PHE295
9	**Tacrine**	−10.59	−54.02	Tyr341, Tyr337 and Trp86
10	**Donepezil**	−10.57	−97.4	TRP286, TRP86, TYR337, PHE338, PHE295 has HBond

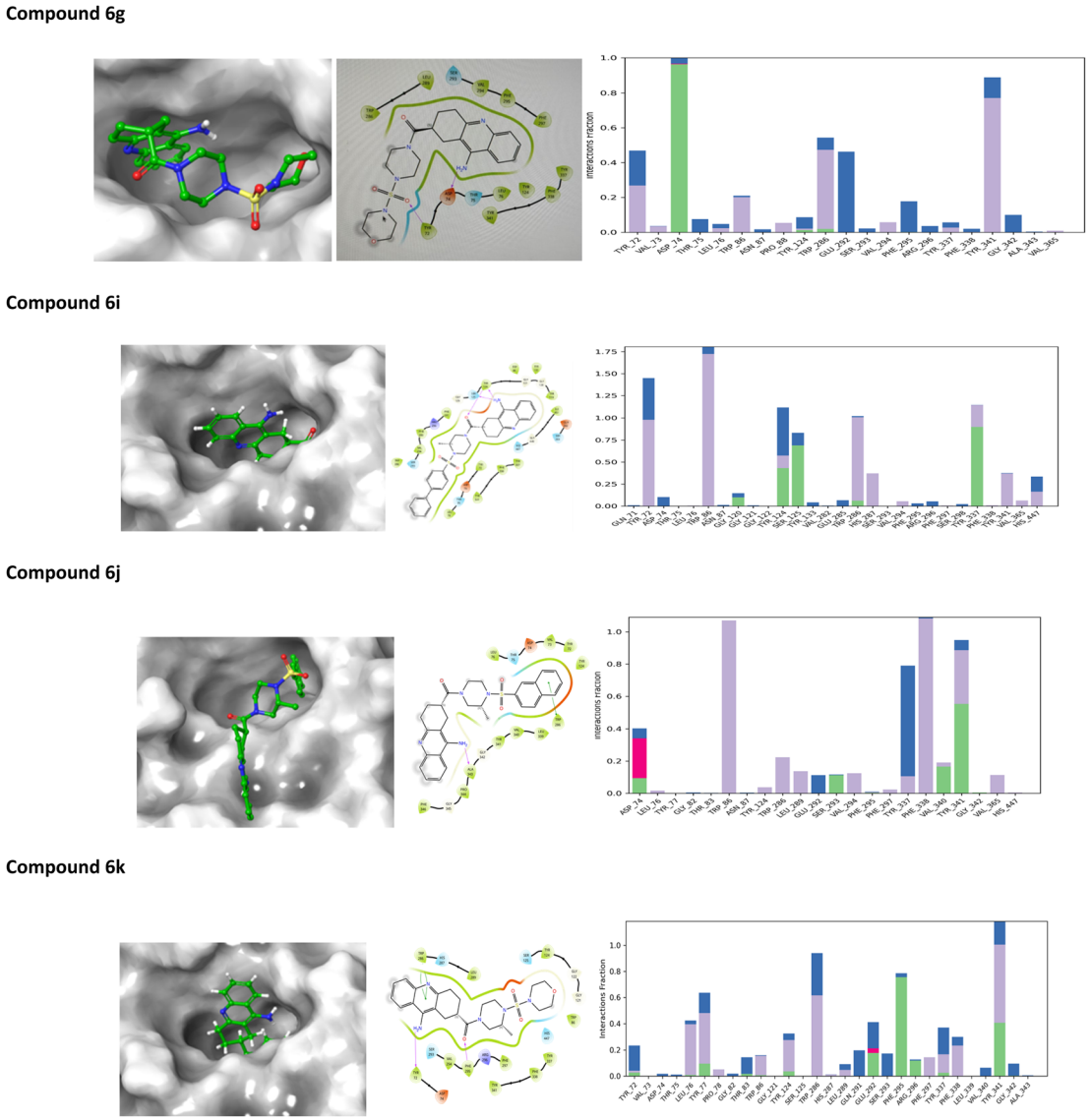

Fig. 3 Binding pattern of synthesized compounds.

and π-cation), hydrogen bonding, and hydrophobic contacts. The designed compounds exhibited interactions with critical residues such as Trp86, Trp286, His447, Phe338, Tyr337, and Tyr341. Among the tested molecules, compounds **6g**, **6i**, **6j**, and **6k** demonstrated the highest binding affinity toward AChE (Fig. 3).

AChE inhibition screening and IC_{50} determination

The synthesized novel tacrine derivatives were evaluated for acetylcholinesterase (AChE) inhibitory activity using Ellman's method. For initial screening, compounds were tested at a concentration of 200 nM (based on an optimized ligand concentration of 208 nM from a prior study) and incubated with the enzyme for 45 minutes before measuring residual activity using the substrate. Percent enzyme activity in the presence of each derivative was calculated relative to the native (no-ligand) control. Inhibition was quantified by plotting absorbance *versus* time, and percent inhibition was determined from the resulting curves. Subsequently, concentration response experiments were conducted to determine IC_{50} values.[40,41]

All tested compounds exhibited potent AChE inhibition, with IC_{50} values in the nanomolar range (Table 2). These biochemical results corroborate the *in silico* binding affinities and support further investigation of the most active derivatives. All synthesized sulphonamide derivatives demonstrated enhanced inhibitory profiles compared to tacrine. The IC_{50} value presented is the mean ± standard deviation of at least three separate experiments. Compound **6a** (*p*-methylphenyl sulphonamide, IC_{50} = 31.39 nM), the strong potency highlights the beneficial role of an electron-donating methyl group. This likely enhances hydrophobic interactions within the active site gorge of AChE, stabilizing binding. Compounds **6b** and **6c** (*p*-/*m*-nitrophenyl sulphonamides, IC_{50} = 412.84 nM and 211.68 nM), the nitro group, being strongly electron-withdrawing,

Table 2 *In vitro* AChE profile of Tacrine derivatives

S. No.	Compound name	AChE IC_{50} (nM)	Modification	Interpretation
1	**6a**	31.39 ± 4.12	Electron-donating methyl	Enhances hydrophobic fit
2	**6b**	412.84 ± 4.46	Electron-withdrawing nitro	Reduces π–π interactions
3	**6c**	211.68 ± 3.64		
4	**6d**	436.07 ± 5.82	Methoxy group	Steric/polar disruption
5	**6e**	356.95 ± 3.12	Unsubstituted phenyl substitution	Baseline activity
6	**6f**	53.01 ± 2.90	Extended aromaticity	Strong π–π stacking
7	**6g**	188.02 ± 1.76	Polar heterocycle	Hydrogen bonding but weaker hydrophobic fit
8	**6h**	53.38 ± 2.62	Methylated piperidine derivatives	The methyl groups on the piperidine ring likely enhance lipophilicity + conformational optimization
9	**6i**	50.76 ± 2.46		
10	**6j**	7.40 ± 1.46		
11	**6k**	11.33 ± 2.26		
12	**Tacrine**	94.69 ± 3.74	NA	NA

reduces electron density on the aromatic ring. This may weaken π–π stacking or hydrophobic interactions with aromatic residues in the enzyme, explaining the reduced potency. Compound **6d** (*p*-methoxyphenyl sulphonamide, IC_{50} = 436.07 nM), despite being electron-donating, the $-OCH_3$ group introduces steric hindrance and polarity that may disrupt optimal binding orientation, leading to weaker inhibition compared to the $-CH_3$ group. The compound **6e** (unsubstituted phenyl sulphonamide, IC_{50} = 356.95 nM), the lack of substituents results in moderate activity, suggesting that substituent-driven electronic and steric effects are key to optimizing potency. The compounds **6f** and **6g** (naphthyl and morpholine sulphonamides, IC_{50} = 53.01 nM and 188.02 nM), the naphthyl group provides extended aromatic surface area, enhancing π–π stacking with aromatic residues in AChE. The morpholine moiety introduces polarity and hydrogen-bonding potential, but at the cost of reduced hydrophobic fit, explaining its weaker activity. The compounds **6h–6k** (methyl-substituted piperidines, IC_{50} = 53.38 nM, 50.76 nM, 7.40 nM, and 11.32 nM respectively), these derivatives show dramatic improvements in potency, especially **6j** (7.40 nM) and **6k** (11.32 nM) is due to the methyl groups on the piperidine ring likely enhance lipophilicity, improving penetration into the hydrophobic active site. They may also enforce conformational rigidity, orienting the sulphonamide moiety for optimal binding. The sharp increase in potency suggests that fine-tuning steric bulk and hydrophobicity on the piperidine scaffold is a highly effective strategy. In summary, the SAR analysis reveals that hydrophobic and steric optimization on the piperidine ring is the most effective strategy for enhancing AChE inhibition, while electron-withdrawing substituents on the sulphonamide moiety reduce potency. This provides a clear roadmap for rational design of next-generation inhibitors.

Correlation between docking scores and IC_{50} values

The docking and biological evaluation of the designed compounds revealed a generally consistent relationship between computational predictions and experimental potency, with notable exceptions. Compound **6j** (Glide score −9.18, binding energy −97.92) exhibited the lowest IC_{50} value of 7.40 nM, demonstrating excellent agreement between strong docking affinity and inhibitory activity. Similarly, compound **6k** (Glide score −6.97, binding energy −90.65) showed robust binding interactions and a low IC_{50} of 11.33 nM, reinforcing the predictive value of docking scores. In contrast, compound **6d** (Glide score −5.29, binding energy −43.25) displayed a markedly higher IC_{50} (436.07 nM), consistent with its weaker docking profile. Compound **6e** (Glide score −1.33, binding energy −64.98) presented a high IC_{50} value of 356.95 nM despite favourable binding energy, suggesting that docking predictions may not fully capture conformational flexibility or solubility effects influencing enzyme inhibition. Compound **6a** (Glide score −5.84, binding energy −47.68) demonstrated a moderate IC_{50} (31.39 nM), aligning reasonably with its computational profile, while compound **6i** (Glide score −3.55, binding energy −81.28) exhibited a comparatively low IC_{50} (50.76 nM), implying that hydrogen bond interactions may compensate for weaker docking scores. Overall, these findings highlight that while docking simulations provide valuable preliminary insights into binding affinity, experimental IC_{50} validation remains essential to account for structural and physicochemical factors not fully captured *in silico* (Fig. 4).

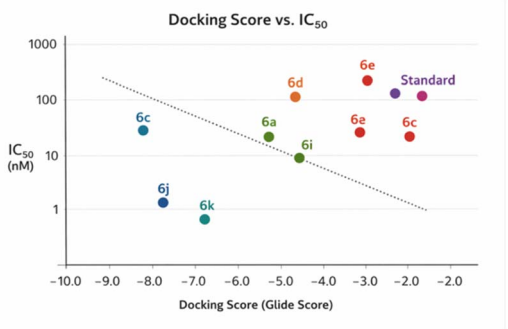

Fig. 4 Docking score *vs.* IC_{50}.

Table 3 ADME properties of synthesized compounds

	CNS	Mol wt	SASA	HBD	HBA	QPPCaco	QP log BB	QPPMDCK	% Of HOA	PSA	QP log HERG	Criteria passed
6a	−2	464.58	770.94	1.5	9.5	243.878	−1.271	178.131	85.996	102.35	−5.111	4
6b	−2	495.55	779.74	1.5	10.5	28.58	−2.41	17.519	63.44	146.9	−5.121	2
6c	−2	495.55	750.1	1.5	10.5	69.66	−1.86	45.435	71.24	338.87	−4.969	1
6d	−2	480.58	777.06	1.5	10.25	242.503	−1.334	177.278	84.70	110.64	−5.134	3
6e	−2	526.65	828.13	1.5	9.5	262.18	−1.28	182.268	82.38	120.68	−5.142	3
6f	−2	500.61	812.49	1.5	9.5	224.03	−1.365	162.55	75.96	101.95	−5.81	2
6g	−2	459.56	728.2	1.5	9.7	183.21	−1.17	183.21	82.92	114.42	−3.848	3
6h	−2	494.61	789.92	1.5	10.25	319.09	−1.22	225.89	88.64	106.06	−4.972	4
6i	−2	540.68	869	1.5	9.5	322.38	−1.31	226.84	84.34	97.21	−6.226	5
6j	−2	514.64	805.56	1.5	9.5	352.64	−1.13	236.91	81.14	95.32	−5.721	5
6k	−2	473.59	728.37	1.5	9.7	291.6	−1.09	204.55	85.09	110.22	−3.899	5

Table 4 *In silico* toxic profiles of the synthesised compounds

Derivative	Hep	Neu	Nep	Res	Car	Can	Imm	Mut	Cyt	BBB	Eco	Cli	Nut	Cho	Cir	Hpt	Sta
6a	✓	✓	✓	☒	✓	✓	✓	✓	✓	☒	✓	☒	✓	☒	☒	✓	☒
6b	✓	✓	✓	☒	✓	☒	✓	☒	✓	☒	✓	✓	✓	☒	☒	✓	☒
6c	✓	✓	✓	☒	✓	☒	✓	☒	✓	☒	✓	✓	✓	☒	☒	✓	☒
6d	✓	✓	✓	☒	✓	✓	✓	✓	✓	☒	✓	☒	☒	☒	☒	✓	☒
6e	✓	☒	✓	☒	✓	✓	✓	✓	✓	☒	✓	☒	✓	☒	☒	✓	☒
6f	✓	✓	✓	☒	✓	✓	✓	✓	✓	☒	✓	☒	✓	☒	☒	✓	☒
6g	✓	✓	✓	☒	✓	✓	✓	✓	✓	☒	✓	☒	✓	☒	☒	✓	☒
6h	✓	✓	✓	☒	✓	✓	✓	✓	✓	☒	✓	☒	✓	☒	☒	✓	☒
6i	✓	☒	✓	☒	✓	✓	✓	✓	✓	☒	✓	☒	✓	☒	☒	✓	☒
6j	✓	✓	✓	☒	✓	✓	✓	✓	✓	☒	✓	☒	✓	☒	☒	✓	☒
6k	✓	✓	✓	☒	✓	✓	✓	✓	✓	☒	✓	☒	✓	☒	☒	✓	☒
Tacrine	✓	☒	✓	☒	✓	✓	☒	✓	✓	☒	☒	☒	✓	☒	✓	✓	☒

Abbreviations: Hep: hepatotoxicity, Neu: neurotoxicity, Nep: nephrotoxicity, Res: respiratory toxicity, Car: cardiotoxicity, Can: carcinogenicity, Imm: immunotoxicity, Mut: mutagenicity, Cyt: cytotoxicity, BBB: BBB-barrier, Eco: ecotoxicity, Cli: clinical toxicity, Nut: nutritional toxicity, Cho: choleostasis, Cir: cirrhosis, Hpt: hepatitis, Sta: steatosis; note: ☒ indicates predicted toxicity (T); ✓ indicates predicted non-toxicity (NT) based on ProTox 3.0 and ToxSTAR platforms.

In silico predictions of physico–chemical properties of the synthesised compounds

The ADME properties of the conformers were predicted using the QikProp module. Accurate prediction of ADME profiles at the early stages of drug development can significantly reduce both the time and cost associated with preclinical and clinical studies. Prior to molecular docking, the ligands were filtered based on their structural and pharmacokinetic characteristics. The drug-like behaviour of the tacrine derivatives was evaluated through *in silico* analysis. Key parameters, including molecular weight (MW), partition coefficient (log *P*), number of hydrogen bond donors (HBD) and acceptors (HBA), polar surface area (PSA), and solvent-accessible surface area (SASA), were assessed and compared with reference values, as summarized in Table 3. All derivatives satisfied the criteria for drug-likeness, conforming to Lipinski's Rule of Five and Jorgensen's Rule of Three. Notably, compounds targeting the central nervous system (CNS) typically exhibit lower values for these parameters compared to drugs acting on peripheral systems.[42–44]

In silico toxic profiles of the synthesised compounds

The *in silico* toxicity profiles of compounds **6a–6k** and the standard were evaluated using ProTox-3.0 and ToxSTAR. Most

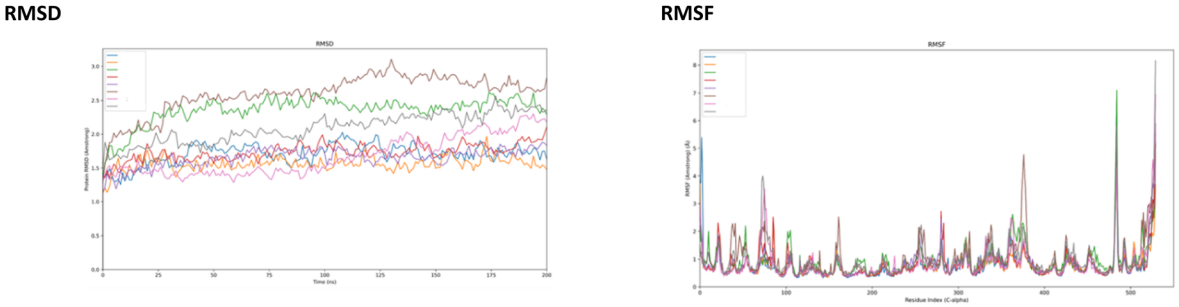

Fig. 5 The RMSD and RMSF graph of Cα (blue in colour), ligand displacement (pink and in colour).

Table 5 Binding free energy of the AChE-derivative

Derivatives	Binding energy	Coulomb	Covalent	Bond	Lipo	Solv_GB
6a	−100.68 ± 5.05	23.68 ± 14.17	4.37 ± 1.78	−1.96 ± 0.48	−28.18 ± 1.51	27.02 ± 15.62
6d	−95.70 ± 5.38	29.07 ± 9.29	3.59 ± 0.79	−1.14 ± 0.60	−28.65 ± 1.00	−21.75 ± 9.95
6e	−52.65 ± 5.11	34.67 ± 17.74	4.18 ± 1.62	−1.54 ± 0.24	−11.15 ± 2.05	−35.28 ± 15.37
6f	−80.86 ± 5.65	18.20 ± 14.21	3.60 ± 2.71	−1.64 ± 0.58	−25.83 ± 2.07	−12.97 ± 14.03
6h	−106.53 ± 9.47	24.49 ± 18.45	6.01 ± 3.07	−1.63 ± 0.34	−31.36 ± 2.38	−21.48 ± 15.83
6i	−51.023 ± 7.49	17.51 ± 22.39	4.55 ± 3.01	−0.864 ± 0.53	−16.09 ± 3.55	−12.37 ± 18.85
6j	−70.17 ± 11.09	19.91 ± 18.67	2.87 ± 1.65	−1.61 ± 0.32	−23.38 ± 3.95	−13.68 ± 18.97

compounds showed similar patterns, with consistent predictions of respiratory toxicity, BBB permeability, and liver-associated toxicities. Compound **6a** was largely inactive except for respiratory toxicity, BBB permeability, and clinical toxicity (Table 4). Compounds **6b** and **6d** raised greater concern due to predicted carcinogenicity and mutagenicity. Compounds **6e** and **6i**, along with the standard, showed additional neurotoxicity or immunotoxicity. Several compounds (**6h**, **6i**, **6k**, and standard) also indicated liver toxicity for cholestasis, cirrhosis, or steatosis, though hepatitis was absent. Overall, risks for hepatotoxicity, nephrotoxicity, cardiotoxicity, cytotoxicity, and mutagenicity were low, but the recurring predictions of respiratory toxicity, BBB permeability, and liver-related effects highlight the need for further experimental validation before therapeutic consideration.

RMSD and RMSF

The binding stability of tacrine derivatives with acetylcholinesterase (AChE) was investigated through molecular dynamics (MD) simulations conducted over 200 ns. Conformational changes in the AChE-ligand complexes during the simulation were analysed using root mean square deviation (RMSD). Larger RMSD deviations indicate significant structural shifts within the AChE, suggesting potential instability of the complex. The average RMSD for the protein in complex with the top-scoring derivatives was found to be 1.87 ± 0.20 Å, indicating overall structural stability. MD results revealed no significant changes in the global structure or binding orientation of the derivatives throughout the simulation.[45,46] The average root mean square fluctuation (RMSF) value for the AChE derivative complex was 0.84 ± 0.56 Å, reflecting stable residue-level flexibility during ligand interaction. RMSF profiles for all complexes are illustrated in Fig. 5. Throughout the MD simulation, the derivatives maintained ionic interactions, hydrogen bonds, and water bridges with key active site residues (Fig. 5). Binding energies were calculated using the MM-GBSA method from selected frames of the MD trajectory. Ten representative frames from the 200 ns simulation were used to estimate the binding free energy of the AChE-derivative complexes. The results are summarized in Table 5.

The seven derivatives are analysed for their conformational changes and binding energy by MD simulation. All showed good binding energy >50 kcal mol^{-1}. Derivatives **6a** and **6i** have binding energy >100 kcal mol^{-1}. Thus, all 7 derivatives were selected for the AChE assay. The binding stability of tacrine derivatives with AChE was studied through molecular dynamics simulation for 200 ns. AChE and corresponding derivatives conformation changes from their initial structures throughout the simulation can be analysed using RMSD. Greater deviations in RMSD suggest a significant conformational shift occurring within the AChE during the simulation, indicating an unstable AChE derivative complex. Average protein RMSD for the AChE and top-scoring derivatives is found to be 1.87 ± 0.20 A°. MD studies indicate that there are no significant changes observed in terms of the overall structure and orientation of derivatives binding during the simulation.

Compound **6h** exhibited the strongest binding energy (−106.53 kcal mol^{-1}), primarily driven by significant lipophilic stabilization (−31.36) and moderate coulombic contributions, suggesting that hydrophobic interactions play a central role in its affinity. Compound **6a** also demonstrated high binding energy (−100.68 kcal mol^{-1}), with balanced coulombic and solvation effects, indicative of stable electrostatic and solvation–

driven interactions. Compound **6d** showed slightly weaker binding (−95.70 kcal mol^{-1}) but with enhanced Coulombic stabilization compared to **6a**, reflecting stronger charge–charge interactions. Compounds **6f** and **6j** displayed moderate binding energies (−80.86 and −70.17 kcal mol^{-1}, respectively), dominated by lipophilic contributions, implying a greater reliance on hydrophobic contacts than electrostatics. In contrast, compounds **6e** and **6i** exhibited the weakest binding energies (−52.65 and −51.02 kcal mol^{-1}), characterized by poor lipophilic stabilization and unfavorable solvation terms, suggesting that these derivatives are likely less potent binders (Table 5).

Conclusions

In this study, we report the synthesis of tacrine–sulphonamide hybrids and their evaluation as acetylcholinesterase (AChE) inhibitors. Methyl-substituted piperidine derivatives exhibited significantly enhanced inhibitory potency, with compounds **6j** ($IC_{50} = 7.40$ nM) and **6k** ($IC_{50} = 11.33$ nM) emerging as the most promising candidates. Computational studies revealed strong binding interactions with key active-site residues, including Trp86, Trp286, Tyr337, and Phe338, mediated by π–π stacking, π-cation interactions, hydrogen bonding, and hydrophobic forces. The sulphonamide derivatives showed stronger inhibition compared to the amide derivatives reported in our previous studies. This enhanced activity may be attributed to the electronic effects of the sulphonyl group, which is more electron-withdrawing than the carbonyl group, thereby increasing hydrogen-bonding potential and modulating polarity. Moreover, sulphonamides often act as stronger hydrogen-bond donors and acceptors than amides, which can improve interactions with both catalytic and peripheral residues in AChE. Overall, these findings demonstrate that tacrine-based sulphonamide derivatives, particularly compounds **6j** and **6k**, are highly potent AChE inhibitors with considerable potential for further therapeutic development.

Experimental section

ADME prediction

The Qikprop module of the Schrodinger program is used to predict the ADME properties of the derivatives. The derivatives are filtered out before docking based on their structural and pharmacokinetic profiles. Features used to filter the derivatives based upon Lipinski rules and other pharmacokinetic parameters, such as percentage of HOA > 80, HBA <10, top 70% of QPPCaco, top 70% of QPPMDCK, molecular weight < 500 dalton, QPlogHERG < −5. The derivatives that pass at least 3 of the features are considered for docking and molecular dynamics simulation.

MD simulations

To investigate the stability and affinity of the derivatives and standard bound AChE complexes, the protein complex with the ligand was subjected to 200 ns MDS using the Desmond module. The built structures were positioned within an orthorhombic box, and TIP3P water molecules were used as solvent in a system with the OPLS 2005 force field. Adequate quantities of Na^+/Cl^- ions were included to neutralize the system. The temperature and pressure were optimized to 300 K and 1 atmosphere, respectively, *via* isotropic scaling (Martyna–Tobias–Klein) and Nose–Hoover temperature coupling. Intermediate structures were preserved every 100 ps for the computation of the subsequent parameters: (i) root mean square deviations (RMSD) of the protein and ligands, (ii) RMSF of proteins and derivatives, (ii) ligand interactions, and (iii) post-MDS MM-GBSA utilizing the thermal.py script.[47]

Acetyl cholinesterase assay

The AMPLITE™ AChE assay kit (AAT Bioquest, Inc., Sunnyvale, CA) was used to identify the *in vitro* inhibitory effects of the newly synthesized tacrine-sulfonyl piperazine derivatives. The assay system is based on Ellman's method.[48] The assay kit contained acetylcholinesterase (AChE) from electric eel (EC 3.1.1.7), assay buffer (pH 7.4), 5,5-dithiobis-2-nitrobenzoic acid (DTNB, known as Ellman's reagent), and the substrate acetylthiocholine (AChT). A 100 mL reaction mixture was prepared by mixing the enzyme (0.3 U), 500 mM AChT solution in ddH_2O, and 500 μM DTNB in the assay buffer. Enzyme activity was determined by measuring the increase in absorbance at 405 nm at 2 minutes intervals at 37 °C for 20 minutes. Tacrine derivatives were dissolved in DMSO and preincubated at room temperature with the enzyme for 20 minutes, followed by the addition of AChT and DTNB. The IC_{50} value, representing the inhibitor concentration required for 50% inhibition, was determined for each derivative by measuring enzyme activity at different inhibitor concentrations over 20 minutes.

Synthesis

All reactions were carried out with commercial grade-solvents. Thin-layer chromatography (TLC) was performed on silica gel plates (60F-254) using UV-light (254 and 365 nm). All intermediates were used without column chromatography purification, whereas final compounds were column purified. NMR (400 MHz for ^1H NMR and ^{13}C NMR) spectra were recorded in DMSO with TMS as the internal standard. Chemical shifts are reported in ppm, and coupling constants are given in Hz. Data for ^1H NMR are recorded as follows: chemical shift (ppm), multiplicity (s, singlet; d, doublet; dd, doublet of doublet; t, triplet; q, quartet; m, multiplet, coupling constant (Hz), and integration. Data for ^{13}C NMR are reported in terms of chemical shift (δ, ppm). High-resolution mass spectra (HRMS) were recorded on Micro Mass ESI-TOF MS.

General procedure for the synthesis

Step-1. To a stirred solution of 1-Boc-piperazine **2** (1.0 eq.) in *N*-methyl-2-pyrrolidone (8.0 vol) was added *N*,*N*-diisopropylethylamine (3.0 eq.) at 0 °C followed by the addition of corresponding sulfonyl chloride **1a–1g** (1.1 eq.) at 0 °C, and then the reaction mass was stirred at room temperature(30–35 °C) for 3 h. The Progress of the reaction was monitored by TLC (mobile phase is pure ethyl acetate, product R_f range is 0.1–0.2). After

completion of the reaction, the reaction mass was diluted with water (40 mL), extracted with ethyl acetate three times. The combined organic layers were dried over sodium sulphate, concentrated at 40 °C and crystallized in hexane to obtain **2a** to **2k** in 70–85% yield.

Step-2. To a stirred solution of compound **3** (1.0 eq.) in dichloromethane (10 vol) at 5–10 °C was added 4 M hydrogen chloride in dioxane (2 vol) and stirred for 3 h at room temperature (30–35 °C). After completion of the reaction, the reaction mixture was concentrated under reduced pressure at 35–38 °C, co-distilled at 40 °C with hexane and filtered to obtain **3a** to **3k**.

Step-3: general procedure for the synthesis of final compounds 6a–6k. To a stirred solution, compound **5** (200 mg, 0.825 mmol, 1.0 eq.) in *N*-methyl-2-pyrrolidone was cooled to 0 °C and *N*,*N*-diisopropylethylamine (213.4 mg, 1.65 mmol, 2.0 eq.), *O*-(benzotriazol-1-yl)-*N*,*N*,*N*′,*N*′-tetramethyluronium tetrafluoroborate (TBTU, 291.6 mg, 0.908 mmol, 1.1 eq.) and the reaction mixture was stirred for 15 min at same temperature. To this reaction mass was added compound **3** (1.1. eq.) and stirred at room temperature (30–35 °C) for 6 h. The reaction mixture was diluted with water and extracted with ethyl acetate twice. The combined organic layers were dried over sodium sulphate, concentrated under reduced pressure at 40 °C and purified by column chromatography (100–200 mesh silica from Avra Laboratories) using 10% methanol in dichloromethane, the TLC mobile phase was 15% methanol in MDC with R_f is 0.3–0.4 range to obtain final compounds **6a–6k**.

*Compound **6a**: (9-amino-1,2,3,4-tetrahydroacridin-2-yl)[4-(p-toluenesulfonyl)piperazin-1-yl]methanone.* Compound **6a** was synthesized in accordance with the typical process by taking a solution of compound **5** (200 mg, 0.825 mmol, 1.0 eq.) was **3** (251.33 mg, 0.908 mmol, 1.1 equiv.) and DIPEA (213.4 mg, 1.65 mmol, 2.0 eq.), TBTU (291.6 mg, 0.908 mmol, 1.10 eq.) in NMP (4 mL). off white colour solid: 72% yield (276 mg); ^{1}H-NMR (400 MHz, DMSO-d_6): δ 8.24 (d, J = 8.4 Hz, 1H, Ar–H), 7.73–7.59 (m, 4H, Ar–H), 7.50 (d, J = 8.0 Hz, 1H, Ar–H), 7.39 (t, J = 7.6 Hz, 1H, Ar–H), 7.22–7.15 (m, 2H, Ar–H), 6.75 (broad Hump s, 2H, NH_2), 3.64 (d, J = 6.0 Hz, 4H, piperazine-CH_2), 3.12–2.85 (m, 8H, piperazine-CH_2 + benzylic-CH_2 + CH), 2.62 (m, 2H, CH_2), 2.42 (s, 3H, Ar–CH_3), 1.90–1.65 (m, 2H, aliphatic CH_2), ^{13}C-NMR (400 MHz, DMSO-d_6): δ 172.8, 154.1, 143.8, 132.0, 129.9, 129.7, 127.6, 123.8, 122.3, 118.2, 116.0, 110.9, 107.8, 46.2, 45.9, 45.8, 45.5, 44.3, 40.4, 35.0, 30.2, 26.3, 24.9, 21.0. HRMS (ESI): calculated for $C_{25}H_{28}N_4O_3S$ [M + H]$^+$: 465.19549; found: 465.19617.

*Compound **6b**: (9-amino-1,2,3,4-tetrahydroacridin-2-yl)(4((4-nitrophenyl)sulfonyl)piperazin-1-yl)methanone.* Compound **6b** was synthesized in accordance with the typical process by taking a solution of **5** (200 mg, 0.825 mmol, 1.0 eq.) was **3** (279.46 mg, 0.908 mmol, 1.1 equiv.) and DIPEA (213.4 mg, 1.65 mmol, 2.0 eq.), TBTU (291.6 mg, 0.908 mmol, 1.10 eq.) in NMP (4 mL). Yellow color solid: 90% yield (368 mg); ^{1}H-NMR (400 MHz, DMSO-d_6): δ 8.48 (d, J = 8.4 Hz, 2H, Ar–H), 8.05–8.01 (m, 2H, Ar–H), 7.61 (d, J = 7.6 Hz, 1H, Ar–H), 7.50 (d, J = 8.0 Hz, 1H, Ar–H), 7.49 (t, J = 7.2 Hz, 2H, Ar–H), 7.29–7.25 (m, 1H, Ar–H), 6.44 (s, 2H, NH_2), 3.69–3.57 (m, 4H, piperazine-CH_2), 3.17–2.80 (m, 6H, piperazine-CH_2 + benzylic-CH_2), 2.79–2.53 (m, 2H, CH + aliphatic CH_2), 1.88 (d, J = 12.0 Hz, 1H, CH_2), 1.74–1.63 (m, 1H, CH_2). ^{13}C-NMR (400 MHz, DMSO-d_6): δ 173.1, 156.2, 150.1, 148.4, 145.9, 140.8, 129.1, 128.1, 127.4, 124.8, 122.7, 121.8, 116.8, 107.5, 46.1, 45.7, 44.3, 40.4, 35.5, 32.2, 26.7, 25.6. HRMS (ESI): calculated for $C_{24}H_{25}N_5O_5S$ [M + H]$^+$: 496.16492; found: 496.16573.

*Compound **6c**: (9-amino-1,2,3,4-tetrahydroacridin-2-yl)(4((2-nitrophenyl)sulfonyl)piperazin-1-yl)methanone.* Compound **6c** was synthesized in accordance with the typical process by taking a solution of **5** (200 mg, 0.825 mmol, 1.0 eq.) was **3** (279.46 mg, 0.908 mmol, 1.1 equiv.) and DIPEA (213.4 mg, 1.65 mmol, 2.0 eq.), TBTU (291.6 mg, 0.908 mmol, 1.10 eq.) in NMP (4 mL). Light yellow color solid 78% yield (319.08 mg. ^{1}H-NMR (400 MHz, DMSO-d_6) δ 8.21–8.19 (d, J = 8.4 Hz, 1H, Ar–H), 8.05–034 (d, J = 7.2 Hz, 2H, Ar–H), 7.96–7.94 (d, J = 9.2 Hz, 2H, Ar–H), 7.88 (t, J = 7.6 Hz, 1H, Ar–H), 7.66 (t, J = 7.6 Hz, 1H, Ar–H), 7.58 (t, J = 7.4 Hz, 1H, Ar–H), 6.75 (br s, 2H, NH_2), 3.71–3.61 (m, 4H, piperazine-CH_2), 3.22–3.12 (m, 4H, piperazine CH_2), 2.96–2.88 (m, 1H, aliphatic CH), 2.68–2.54 (m, 4H, aliphatic 2 × CH_2), 1.98–1.75 (m, 2H, aliphatic CH_2). ^{13}C-NMR (400 MHz,DMSO-d_6): δ 173.1, 147.9, 135.0, 132.5, 130.5, 129.3, 129.0, 125.6, 124.3, 123.4, 122.2, 116.4, 107.8, 46.0, 45.7, 44.7, 40.9, 35.3, 31.0, 26.6, 25.2. HRMS (ESI): calculated for $C_{24}H_{25}NO_5S$ [M + H]$^+$: 496.16492; found: 496.16561.

*Compound **6d**: (9amino1,2,3,4tetrahydroacridin2-yl)(4((4-methoxyphenyl)sulfonyl)piperazin-1-yl)methanone.* Compound **6d** was synthesized in accordance with the typical process by taking a solution of **5** (200 mg, 0.825 mmol, 1.0 eq.) was **3** (265.86 mg, 0.908 mmol, 1.1 equiv.) and DIPEA (213.4 mg, 1.65 mmol, 2.0 eq.), TBTU (291.6 mg, 0.908 mmol, 1.10 eq.) in NMP (4 mL).Off white colour solid 90% yield (357.0 mg); ^{1}H-NMR (400 MHz, DMSO-d_6): δ 8.15 (d, J = 8.0 Hz, 1H, Ar–H), 7.72–7.68 (m, 2H, Ar–H), 7.62 (d, J = 8.0 Hz, 1H, Ar–H), 7.50 (t, J = 8.0 Hz, 1H, Ar–H), 7.29 (t, J = 8.0 Hz, 1H, Ar–H), 7.20–7.16 (m, 2H, Ar–H), 6.51 (s, 2H, NH_2), 3.87 (s, 3H, OCH_3), 3.65 (m, 4H, piperazine-CH_2), 2.99–2.80 (m, 8H, piperazine-CH_2 + benzylic-CH_2 + CH), 1.95–1.64 (m, 4H, aliphatic CH_2), ^{13}C-NMR (400 MHz, DMSO-d_6): δ 173.1, 162.9, 155.9, 148.7, 129.8, 128. 4, 126.3122.9121.9116.7114.6107.6, 55.7, 46.3, 45.8, 44.3, 40.4, 35.5, 31.9, 26.7, 25.6. HRMS (ESI): calculated for $C_{25}H_{28}N_4O_4S$ [M + H]$^+$: 481.19040; found: 481.19152.

*Compound **6e**: (4-([1,1′-biphenyl]-4-ylsulfonyl)piperazin-1-yl)(9-amino-1,2,3,4-tetrahydroacridin-2-yl)methanone.* Synthesized from **5** (200 mg, 0.825 mmol, 1.0 eq.), was **3** (306.78 mg, 0.908 mmol, 1.1 equiv.), DIPEA (213.4 mg, 1.65 mmol, 2.0 eq.), and TBTU (291.6 mg, 0.908 mmol, 1.10 eq.) in NMP (4 mL). Off-white solid: 75% yield (326 mg). ^{1}H-NMR (400 MHz, DMSO-d_6): δ 8.42–8.40 (d, J = 8.4 Hz, 1H, Ar–H), 7.98–7.96 (d, J = 8.0 Hz, 2H, Ar–H), 7.89–7.87 (d, J = 8.4 Hz, 2H, Ar–H), 7.84–7.76 (m, 2H, Ar–H), 7.63–7.52 (m, 4H, Ar–H), 7.49–7.39 (m, 2H, Ar–H), 7.35 (br s, 2H, NH_2), 3.71–3.61 (m, 4H, piperazine-CH_2), 3.15–2.92 (m, 5H, piperazine-CH_2 and aliphatic-CH), 2.67–2.55 (m, 4H, aliphatic 2 × CH_2), 1.99–1.72 (m, 2H, aliphatic CH_2). ^{13}C-NMR (400 MHz, DMSO-d_6): δ 172.2, 155.0, 150.8, 142.8, 138.2, 132.9, 129.2, 128.7, 128.4, 128.2, 127.6, 127.1, 125.6, 125.5, 123.6, 114.7, 46.2, 45.8, 44.3, 44.1, 43.0, 34.3, 27.1, 25.6. HRMS (ESI): calcd for $C_{30}H_{31}N_4O_3S$ [M + H]$^+$: 527.21114; found: 527.21217.

*Compound **6f**: (9-amino-1,2,3,4-tetrahydroacridin-2-yl)(4-(naphthalen-2-ylsulfonyl)piperazin-1-yl)methanone.* Synthesized from **5** (200 mg, 0.825 mmol, 1.0 eq.), **3** (283.14 mg, 0.908 mmol, 1.1 equiv.), DIPEA (213.4 mg, 1.65 mmol, 2.0 eq.), and TBTU (291.6 mg, 0.908 mmol, 1.10 eq.) in NMP (4 mL). Off-white solid: 80% yield (331 mg). ^{1}H-NMR (400 MHz, DMSO-d_6): δ 8.48–8.39 (d, J = 7.6 Hz, 1H, Ar–H), 8.39 (s, 1H, Ar–H), 8.22–8.21 (d, J = 4.4 Hz, 1H, Ar–H), 8.11–8.09 (d, J = 8.0 Hz, 2H, Ar–H), 7.91–7.73 (m, 4H, Ar–H), 7.64–7.54 (m, 2H, Ar–H), 7.33 (br s, 2H, NH_2), 3.69–3.61 (m, 4H, piperazine CH_2), 3.10–2.90 (m, 5H, piperazine-CH_2 and aliphatic CH), 2.62–2.54 (m, 4H, aliphatic 2 × CH_2), 1.92–1.69 (m, 2H, aliphatic CH_2). ^{13}C-NMR (400 MHz, DMSO-d_6): δ 172.2, 154.8, 150.9, 142.8, 137.4, 134.5, 132.8, 132.2, 129.5, 129.4, 129.1, 128.8, 127.9, 127.7, 125.8, 125.4, 123.7, 123.0, 122.8, 114.7, 108.2, 48.4, 46.2, 45.9, 45.5, 34.3, 27.2, 25.7. HRMS (ESI): calcd for $C_{28}H_{28}N_4O_3S$ [M + H]$^+$: 501.19549; found: 501.19666.

*Compound **6g**: (9-amino-1, 2, 3, 4-tetrahydroacridin-2-yl)(4-(morpholinosulfonyl)piperazin-1-yl)methanone.* Compound **6g** was synthesized in accordance with the typical process by taking a solution of **5** (200 mg, 0.825 mmol, 1.0 eq.) was **3** (245.87 mg, 0.908 mmol, 1.1 equiv.) and DIPEA (213.4 mg, 1.65 mmol, 2.0 eq.), TBTU (291.6 mg, 0.908 mmol, 1.10 eq.) in NMP (4 mL). Light brown color liquid 80% yield (303.50 mg). ^{1}H-NMR (400 MHz, DMSO-d_6): δ 8.42 (d, J = 8.4 Hz, 1H, Ar–H), 8.14 (s, 1H, Ar–H), 7.84 (t, J = 8.0 Hz, 1H, Ar–H), 7.77 (d, J = 8.0 Hz, 1H, Ar–H), 7.58 (t, J = 7.6 Hz, 1H, Ar–H), 3.67–3.60 (m, 8H, morpholine-OCH_2 + piperazine-CH_2), 3.28–2.96 (m, 11H, morpholine-*N*-CH_2 + piperazine-CH_2 + benzylic-CH_2 + CH), 2.74–2.60 (m, 2H, CH_2), 2.04–1.77 (m, 2H, CH_2). ^{13}C-NMR (400 MHz, DMSO-d_6): δ 172.3, 154.6, 151.3, 137.9, 132.7, 125.3, 123.0, 119.9, 114.9, 108.3, 65.7, 46.5, 46.2, 46.0, 44.8, 41.0, 34.5, 27.6, 25.8, 23.9. HRMS (ESI): calculated for $C_{22}H_{29}N_5O_4S$ [M + H]$^+$: 460.20130; found: 460.20227.

*Compound **6h**: (9-amino-1, 2, 3, 4-tetrahydroacridin-2-yl)(4-((4-methoxyphenyl)sulfonyl)-3-methylpiperazin-1-yl)methanone.* Compound **6h** was synthesized in accordance with the typical process by taking a solution of **5** (200 mg, 0.825 mmol, 1.0 eq.) was **3** (277.69 mg, 0.908 mmol, 1.1 equiv.) and DIPEA (213.4 mg, 1.65 mmol, 2.0 eq.), TBTU (291.6 mg in NMP(4 mL). 0.908 mmol, 1.10 eq.) in NMP (4 mL). Off white color solid 80% yield (326.65 mg). ^{1}H-NMR (400 MHz, DMSO-d_6): δ 8.37 (1H, d, J = 7.6, Ar–H), 7.99 (2H, s, NH_2), 7.53 (1H, d, J = 8.4, Ar–H), 7.15–7.09 (2H, m, Ar–H), 4.24–3.98 (2H, m, piperazine protons-CH_2), 3.84 (3H, s, OCH_3), 3.58 (6H, t, J = 11.6, piperazine methylene protons CH_2), 3.05–2.96 (1H, m, CH), 2.75–2.60 (2H, m, CH_2), 2.10 (3H, s, piperazine methyl protons-CH_3), 1.19–1.15 (4H, m, CH_2); HRMS (ESI): calculated for $C_{26}H_{30}N_4O_4S$ [M + H]$^+$: 495.20605; found: 495.20732.

*Compound **6i**: (4-([1,1-biphenyl]-4-ylsulfonyl)-3-methylpiperazin-1-yl)(9-amino-1,2,3,4-tetrahydroacridin-2-yl)methanone.* Compound **6i** was synthesized in accordance with the typical process by taking a solution of **5** (200 mg, 0.825 mmol, 1.0 eq.) was **3** (319.52 mg, 0.908 mmol, 1.1 equiv.) and DIPEA (213.4 mg, 1.65 mmol, 2.0 eq.), TBTU (291.6 mg, 0.908 mmol, 1.10 eq.) in NMP (4 mL). Off white color solid 78% yield (225.80 mg); ^{1}H-NMR (400 MHz, DMSO-d_6): δ 8.13 (1H, t, J = 6.8, Ar–H), 7.90 (2H, s, NH_2), 7.76 (2H, d, J = 8.0, Ar–H), 7.61 (1H, d, J = 8.4, Ar–H), 7.53–7.43 (6H, m, Ar–H), 7.27 (1H, d, J = 7.2, Ar–H), 6.44 (3H, s, piperazine CH and CH_2), 4.34–4.17 (3H, m, CH_2), 3.67 (1H, d, J = 9.6, CH), 3.22–3.04 (3H, m, CH_2), 2.93–2.83 (2H, m, CH_2), 2.76–2.56 (3H, m, CH), 1.98 (3H, s, piperazine-CH_3), 1.06–0.91 (4H, m, CH_2).^{13}C-NMR (400 MHz, DMSO-d_6): δ 174.0, 173.9, 173.7, 156.4, 148.3, 146.1, 144.3, 138.9, 138.2, 129.2, 128.6, 127.7, 127.5, 127.1, 121.9, 107.6, 107.5, 49.2, 49.1, 45.6, 45.5, 44.6, 35.6, 32.3, 27.0, 26.6, 26.2,14.6,14.2,14.0. HRMS (ESI): calculated for $C_{31}H_{32}N_4O_3S$ [M + H]$^+$: 541.22679; found: 541.22806.

*Compound **6j**: (9-amino-1,2,3,4-tetrahydroacridin-2-yl)(3-methyl-4-(naphthalen-2-yl)sulfonyl)piperazin-1-yl)methanone.* Compound **6j** synthesized from **5** (200 mg, 0.825 mmol, 1.0 eq.), **3** (295.87 mg, 0.908 mmol, 1.1 equiv.), DIPEA (213.4 mg, 1.65 mmol, 2.0 eq.), and TBTU (291.6 mg, 0.908 mmol, 1.10 eq.) in NMP (4 mL). Light brown solid: 82% yield (348 mg). ^{1}H-NMR (400 MHz, DMSO-d_6): δ 8.54 (s, 1H, Ar–H), 8.22–8.20 (d, J = 8.0 Hz, 1H, Ar–H), 8.16–8.13 (d, J = 7.6 Hz, 2H, Ar–H), 7.88–7.85 (m, 1H, Ar–H), 7.76–7.67 (m, 4H, Ar–H), 7.50–7.46 (m, 2H, Ar–H), 6.40 (br s, 2H, NH_2), 4.24–4.21 (m, 1H, piperazine CH), 3.73–3.62 (m, 3H, piperazine CH_2), 3.10–2.66 (m, 8H, piperazine CH2, aliphatic CH and aliphatic 2 × CH_2), 2.04–1.85 (m, 2H, aliphatic-CH_2), 1.04 (s, 3H,CH_3);^{13}C NMR (400 MHz, DMSO-d_6): δ 156.4, 156.3, 148.2, 146.1, 134.3, 131.8, 129.7, 129.3, 128.9, 128.0, 127.9, 127.8, 127.7, 122.6, 122.3, 121.8, 116.8, 49.2, 49.0, 48.9, 32.3, 22.8, 14.6, 14.2, 14.1, 7.9, 7.7. HRMS (ESI): calcd for $C_{29}H_{30}N_4O_3S$ [M + H]$^+$: 515.21114; found: 515.21232.

*Compound **6k**: (9 amino 1,2,3,4 tetrahydroacridin 2-yl)(3 methyl4 (morpholinosulfonyl)piperazin1-yl)methanone.* Compound **6k** was synthesized in accordance with the typical process by taking a solution of **5** (200 mg, 0.825 mmol, 1.0 eq.) was **3** (258.60 mg, 0.908 mmol, 1.1 equiv.) and DIPEA (213.4 mg, 1.65 mmol, 2.0 eq.), TBTU (291.6 mg, 0.908 mmol, 1.10 eq.) in NMP (4 mL). Light brown color liquid 80% yield (312.76 mg); ^{1}H-NMR (400 MHz, DMSO-d_6): δ 8.23–8.14 (m, 1H, Ar–H), 7.64 (d, J = 8.4 Hz, 1H, Ar–H), 7.52 (t, J = 7.6 Hz, 1H, Ar–H), 7.31 (t, J = 6.8 Hz, 1H, Ar–H), 6.62 (s, 2H, NH_2), 4.33 (m, 1H, CH), 3.95–3.87 (m, 2H, CH_2), 3.65–3.63 (m, 4H, morpholine-CH_2), 3.44–3.37 (m, 2H, CH_2), 3.20–3.11 (m, 2H, benzylic protons-CH_2), 3.00–2.94 (m, 3H, CH and CH_2), 2.78–2.62 (m, 6H, methylene protons-CH_2), 1.24–1.14 (m, 3H, methyl group-CH_3).^{13}C-NMR (400 MHz, DMSO-d_6): δ 173.8, 173.6, 155.8, 149.0, 128.5, 126.9, 125.3, 123.0, 116.7, 107.5, 65.5, 49.6, 45.9, 45.6, 449, 41.0, 40.4, 35.7, 31.8, 25.7, 15.0, 14.5, 14.4. HRMS (ESI): calculated for $C_{23}H_{31}N_5O_4S$ [M + H]$^+$: 474.21695; found: 474.21806.

Author contributions

MMR, EKR and VSNK have contributed to the synthetic work and data analysis. AJ and Radul R Dev have contributed to the docking analysis and ADME analysis. SA has contributed ideology and concept.

Conflicts of interest

There are no conflicts to declare.

Data availability

A data availability statement (DAS) is required to be submitted alongside all articles. Please read our full guidance on data availability statements for more details and examples of suitable statements you can use.

Supplementary information (SI) is available. See DOI: https://doi.org/10.1039/d6ra00900j.

Acknowledgements

SA greatly acknowledges ANRF (*i.e.* formerly DST-SERB) for providing financial support under TARE (TAR/2022/000207). The authors MMR, EKR and VSNK thankful to VFSTR for providing the infrastructure to conduct the research work. The author MMR is thankful to Neuland for providing NOC and extensive support.

References

1 World Health Organization, *Dementia*, Fact Sheet, 2024. Available at: https://www.who.int/en/news-room/fact-sheets/detail/dementia.

2 N. Liu, A. Haziyihan, W. Zhao, Y. Chen and H. Chao, *Transl. Neurodegener.*, 2024, **13**, 42.

3 U. Sehar, P. Rawat, A. P. Reddy, J. Kopel and P. H. Reddy, *Int. J. Mol. Sci.*, 2022, **23**, 12924.

4 (*a*) D. Puzzo and O. Arancio, *J. Alzheimers Dis.*, 2012, **33**, S111–S120; (*b*) V. Tumiatti, A. Minarini, M. L. Bolognesi, A. Milelli, M. Rosini and C. Melchiorre, *Curr. Med. Chem.*, 2010, **17**, 1825–1838.

5 S. Long, C. Benoist and W. Weidner, World Alzheimer Report 2023: Reducing dementia risk: never too early, never too late, *Int. J. Alzheimers Dis.*, 2023.

6 (*a*) D. Munos-Torrero, *Curr. Med. Chem.*2008, **15**, 2433–2455; (*b*) G. Pepeu, M. G. Giovannini, *Curr. Alzheimer Res.*, 2009, **6**, 86–96; (*c*) M. Rosini, A. Milelli, C. Tumiatti, V. Andrisano, M. Bartolini, C. Caprini, M. L. Bolognesi and C. Melchiorre, *Curr. Alzheimer Res.*, 2009, **6**, 86–96.

7 D. M. Quinn, Acetylcholinesterase: Enzyme structure, reaction dynamics, and virtual transition states, *Chem. Rev.*, 1987, **87**, 955–979.

8 (*a*) M. K. Hu, L. J. Wu, G. Hsiao and M. H. Yen, *J. Med. Chem.*, 2002, **45**, 2277–2282; (*b*) P. Camps, X. Formosa, C. Galdeano, D. Munoz-Torrero, L. Ramírez, E. Gomez, N. Isambert, R. Lavilla, A. Badia, M. V. Clos and M. Bartolini, *J. Med. Chem.*, 2009, **52**, 5365–5379.

9 S. S. K. Leon, *Pharmaceuticals*, 2011, **4**, 382–418.

10 (*a*) B. Dogga, G. Sravya, S. K. S. Sriram, S. S. S. J. Rao, V. R. Pasupuleti and G. S. G. R. Naidu, *Eur. J. Med. Chem. Rep.*, 2022, **6**, 100094; (*b*) M. I. Fernández-Bachiller, C. Perez, N. E. Campillo, J. A. Paez, G. C. Gonzalez-Munoz, P. Usan, E. Garcia-Palomero, M. G. Lopez, M. Villarroya, A. G. García, A. Martínez and M. I. Rodriguez-Franco, *ChemMedChem*, 2009, **4**, 828–841; (*c*) D. Alonso, I. Dorronsoro, L. Rubio, P. Munoz, E. García-Palomero, M. Del Monte, A. Bidon-Chanal, M. Orozco, F. J. Luque, A. Castro, M. Medina and A. Martinez, *Bioorg. Med. Chem.*, 2005, **13**, 6588–6597; (*d*) F. Mao, L. Huang, L. Luo, W. Liu, L. Lu, Z. Xie and X. Li, *Bioorg. Med. Chem. Lett.*, 2012, **22**, 6498–6502; (*e*) S. Rizzo, B. Rampa, F. Belluti, M. Bartolini, V. Andrisano, A. Cavalli, M. Recanatini and A. Minarini, *J. Med. Chem.*, 2010, **53**, 4927–4937; (*f*) P. J. G. G. J. C. M. S. de Oliveira, *Neuropharmacology*, 2012, **62**, 997–1003; (*g*) P. R. Carlier, Y. F. Han, D. M. Chow, C. P. L. Hok, K. M. Choi, J. K. Wong, J. H. M. Ip and Y. P. Pang, *Bioorg. Med. Chem.*, 1999, **7**, 351–357; (*h*) L. Pourabdi, M. Khoobi, H. Nadri, A. Moradi, F. H. Moghadam, S. Emami, M. M. Mojtahedi, I. Haririan, H. Forootanfar, A. Ameri, A. Foroumadi and A. Shafiee, *Eur. J. Med. Chem.*, 2016, **123**, 298–308; (*i*) F. Mao, L. Huang, G. Sun, S. Hu, J. J. S. Zhou, Z. Li, Q. Ju, X. Wang and X. Li, *Eur. J. Med. Chem.*, 2016, **121**, 758–772; (*j*) L. Costanzo, M. De Franco, M. L. Bolognesi and M. Rosini, *Eur. J. Med. Chem.*, 2013, **62**, 556–563; (*k*) M. Rosini, E. Simoni, M. Caporaso, M. Bartolini, J. J. S. Tarozzi, A. Cavalli, V. Andrisano and M. L. Bolognesi, *J. Med. Chem.*, 2014, **57**, 8576–8589; (*l*) L. Piazzi, A. Cavalli, F. Colizzi, F. Belluti, M. Bartolini, F. Mancini, V. Andrisano, M. Recanatini and B. Rampa, *J. Med. Chem.*, 2008, **51**, 713–716; (*m*) C. Remya, K. V. Dileep, E. Koti Reddy, K. Mantosh, K. Lakshmi, R. Sarah Jacob, A. S. S. Prasad, K. S. J. Prakash and C. Sadasivan, *Comput. Struct. Biotechnol. J.*, 2021, **19**, 4517–4537.

11 (*a*) D. J. Ames, P. S. Bhathal, B. M. Davies and J. R. E. Fraser, *Lancet*, 1988, **1**, 887; (*b*) P. B. Watkins, H. J. Zimmerman, M. J. Knapp, S. I. Gracon and K. W. Lewis, *JAMA*, 1994, **271**, 992–998.

12 S. Mitra, M. Muni, N. J. Shawon, R. Das, T. B. Emran, R. Sharma, D. Chandran, F. Islam, M. J. Hossain, S. Z. Safi and S. H. Sweilam, *Oxid. Med. Cell. Longev.*, 2022, 7252882.

13 F. Queda, S. Calò, K. Gwizdala, J. D. Magalhães, S. M. Cardoso, S. Chaves, L. Piemontese and M. A. Santos, *Molecules*, 2021, **26**, 1658.

14 S. S. Nilewar, *Int. J. Mol. Sci.*, 2026, **27**, 3286.

15 K. Karaman, G. Ş. S. Dokumaci, S. G. Öztürk, H. S. S. Altun, A. S. Önal, O. S. O. Kurt and M. S. M. Ateş, *RSC Adv.*, 2021, **11**, 31234–31245.

16 O. M. Al-Saad, M. Gabr, S. S. Darwish, M. Rullo, L. Pisani, D. V. Miniero, G. M. Liuzzi, A. M. Kany, A. K. H. Hirsch, A. H. Abadi, M. Engel, M. Catto and M. Abdel-Halim, *Eur. J. Med. Chem.*, 2024, **269**, 116266.

17 T. J. Eckroat, D. L. Manross and S. C. Cowan, *Int. J. Mol. Sci.*, 2020, **21**, 5965.

18 K. V. Dileep, K. Ihara, C. Mishima-Tsumagari, M. Kukimoto-Niino, M. Yonemochi, K. Hanada, M. Shirouzu and K. Y. Zhang, *Int. J. Biol. Macromol.*, 2022, **210**, 172–181.

19 L. Arrué, A. Cigna-Méndez, T. Barbosa, P. Borrego-Muñoz, S. Struve-Villalobos, V. Oviedo, C. Martínez-García,

A. Sepúlveda-Lara, N. Millán, J. C. Márquez Montesinos and J. Muñoz, *Pharmaceutics*, 2022, **14**, 1914.
20 H. M. Ragab, M. Teleb, H. R. Haidar and N. Gouda, *Bioorg. Chem.*, 2019, **86**, 557–568.
21 G. Li, G. Hong, X. Li, Y. Zhang, Z. Xu, L. Mao, X. Feng and T. Liu, *Eur. J. Med. Chem.*, 2018, **148**, 238–254.
22 C. N. Patel, A. Shakeel, R. Mall, K. M. Alawi, I. V. Ozerov, A. Zhavoronkov and F. Castiglione, *Wiley Interdiscip. Rev.: Comput. Mol. Sci.*, 2025, **15**, e70004.
23 M. Przybyłowska, S. Kowalski, K. Dzierzbicka and I. Inkielewicz-Stepniak, *Curr. Neuropharmacol.*, 2019, **17**, 472–490.
24 Y. Guo, H. Yang, Z. Huang, S. Tian, Q. Li, C. Du, T. Chen, Y. Liu, H. Sun and Z. Liu, *Molecules*, 2020, **25**, 489.
25 H. Pashaei, A. Rouhani, M. Nejabat, F. Hadizadeh, S. Mirzaei, H. Nadri, M. F. Maleki and R. Ghodsi, *J. Mol. Struct.*, 2021, **1244**, 130919.
26 M. S. Kohnehshahri, G. Chehardoli, M. Bahiraei, T. Akbarzadeh, A. Ranjbar, A. Rastegari and Z. Najafi, *Mol. Divers.*, 2022, **26**, 489–503.
27 S. Mak, W. Li, H. Fu, J. Luo, W. Cui, S. Hu, Y. Pang, P. R. Carlier, K. W. Tsimi, R. Pi and Y. Han, *J. Neurochem.*, 2021, **158**, 1381–1393.
28 M. M. Reddy, A. J, E. K. Reddy, S. Anwar and S. C., *Org. Biomol. Chem.*, 2025, **23**, 6773–6784.
29 E. K. Reddy, C. Remya, K. Mantosh, A. M. Sajith, R. V. Omkumar, C. Sadasivan and S. Anwar, *Eur. J. Med. Chem.*, 2017, **139**, 367–377.
30 B. Dogga, K. Eeda, C. Sharanya, A. J. Jayanandan, A. Gangadharan, C. S. Kumar and K. S. Rangappa, *Eur. J. Med. Chem. Rep.*, 2022, **6**, 100094.
31 C. Remya, K. V. Dileep, E. K. Reddy, K. Mantosh, K. Lakshmi, R. S. Jacob and R. V. Omkumar, *Comput. Struct. Biotechnol. J.*, 2021, **19**, 4517–4537.
32 A. Babu, M. John, M. J. Liji, E. Maria, S. J. Bhaskar, B. K. Binukmar, A. M. Sajith, E. K. Reddy, K. V. Dileep and K. Sunil, *Comput. Biol. Med.*, 2023, **155**, 106666.
33 E. K. Reddy, C. Remya, A. M. Sajith, K. V. Dileep, C. Sadasivan and S. Anwar, *RSC Adv.*, 2016, **6**, 77431–77439.
34 J. Cheung, M. J. Rudolph, F. Burshteyn, M. S. Cassidy, E. N. Gary, J. Love, M. C. Franklin and J. J. Height, *J. Med. Chem.*, 2012, **55**, 10282–10286.
35 (*a*) C. Remya, K. V. Dileep, I. Tintu, E. J. Variyar and C. Sadasivan, *Med. Chem. Res.*, 2012, **21**, 2779–2787; (*b*) A. C. Lalu, B. B. Joseph, T. K. Varun, A. Thaikkad, L. Dcunha, R. Raju and A. Jayanandan, *J. Mol. Graph. Model.*, 2023, **143**, 109262.
36 A. Basiri, M. Xiao, A. McCarthy, D. Dutta, S. N. Byrareddy and M. Conda-Sheridan, *Bioorg. Med. Chem. Lett.*, 2017, **27**, 228–231.
37 Y. Wang, H. Wang and H. Z. Chen, *Curr. Neuropharmacol.*, 2016, **14**, 364–375.
38 M. Junaid, N. Islam, M. K. Hossain, M. O. Ullah and M. A. Halim, *PLoS One*, 2019, **14**, e0211935.
39 S. Jana, A. Ganeshpurkar and S. K. Singh, *Org. Biomol. Chem.*, 2018, **16**, 9477–9495.
40 BenchChem Technical Support Team, *BenchChem Application Note*, 2025, November.
41 C. A. Lipinski, F. Lombardo, B. W. Dominy and P. J. Feeney, *Adv. Drug Deliv. Rev.*, 1997, **23**, 3–25.
42 W. L. Jorgensen and E. M. Duffy, *Adv. Drug Deliv. Rev.*, 2002, **54**, 355–366.
43 H. Pajouhesh and G. R. Lenz, *NeuroRx*, 2005, **2**, 541–553.
44 M. Karplus and J. A. McCammon, *Nat. Struct. Biol.*, 2002, **9**, 646–652.
45 S. A. Hollingsworth and R. O. Dror, *Neuron*, 2018, **99**, 1129–1143.
46 A. Hospital, J. R. Goñi, M. Orozco and J. L. Gelpí, *Adv. Appl. Bioinform. Chem.*, 2015, **8**, 37–47.
47 L. Dcunha, S. D. Thomas, L. John, A. Thaikkad, D. Francis, R. Raju, N. Hirani and A. Jayanandan, *Comput. Biol. Med.*, 2026, **200**, 111372.
48 G. L. Ellman, K. D. Courtney, V. Andres Jr and R. M. Featherstone, A new and rapid colorimetric determination of acetylcholinesterase activity, *Biochem. Pharmacol.*, 1961, **7**, 88e95.